Submitted to: *J. Phys. D: Appl. Phys.*

Atomistic simulations of field assisted evaporation in atom probe tomography

S. Parviainen[1], F. Djurabekova[1], S. P. Fitzgerald[2], A. Ruzibaev[1] and K. Nordlund[1]

[1] Department of Physics and Helsinki Institute of Physics - P.O. Box 43, FIN-00014 University of Helsinki, Finland

[2] Department of Materials, University of Oxford, Parks Road, Oxford, OX1 3PH, UK

E-mail: `stefan.parviainen@iki.fi`

Abstract. Atom probe tomography (APT) is a extremely powerful technique for determining the three-dimensional structure and chemical composition of a given sample. Although it is designed to provide images of material structure with atomic scale resolution, reconstruction artifacts, well-known to be present in reconstructed images, reduce their accuracy. No existing simulation technique has been able to fully describe the origin of these artifacts. Here we develop a simulation technique which allows for atomistic simulations of the atom emission process in the presence of high electric fields in APT experiments. Our code combines hybrid concurrent electrodynamics - molecular dynamics and a Monte Carlo approach. We use this technique to demonstrate the atom-level origin of artifacts in APT image reconstructions on examples of inclusions and voids in investigated samples. The results show that even small variations in the surface topology give rise to distortions in the local electric field, limiting the accuracy of conventional APT reconstruction algorithms.

1. Introduction

Atom probe tomography (APT) is a powerful technique for determining the structure and chemical composition of a sample in three dimensions. The technique has successfully been used to study e.g. multilayer structures [1, 2, 3, 4], clustering in alloys [5, 6, 7, 8] and dopant mapping in semiconductor components [9, 10, 11].

APT is based on the controlled evaporation of atoms ionized by a high electric field (~ 10V/nm) from the studied specimen held at cryogenic temperature. The evaporated ions are accelerated by the applied electric field towards a detector, where their impact time and position are recorded. One way to ensure high detector efficiency is to ensure that only a single ion at a time is evaporated from the sample, which is achieved by pulsing the applied voltage [12] or the sample temperature by means of short laser pulses [13]. Despite this, it is known that multiple simultaneous evaporations and evaporation of dimers and complex molecules still occur [14, 15, 16], requiring advanced detectors to compensate for these kinds of events [17].

In this paper we develop a novel atom-level technique which combines the concurrent electrodynamics-molecular dynamics (HELMOD) code [18] and a Monte Carlo (MC) algorithm to reach beyond the time scales achievable in molecular dynamics (MD) methods. The HELMOD allows the atoms to "feel" the effect of electric field and move accordingly, and the MC step, concurrently incorporated in the MD algorithm, simulates the evaporation process at cryogenic temperature. In this manner, we can simulate directly the field-assisted evaporation of atoms from the surface of a metal needle-shaped specimen, self-consistently modifying the shape of the specimen due to atom evaporation and surface relaxation processes (atoms on the surface moving slightly to minimize surface energy).

The ultimate goal in APT is to be able to reconstruct the studied samples with atomic resolution. However, current APT techniques still result in reconstruction artifacts [19], i.e. some atoms are misplaced in the reconstructed volume. While significant progress has been made in recent years, including increased detector efficiency and accuracy, algorithms for lattice rectification and compensation for undetected atoms [20, 21], and improved crystallographic structure analysis [22, 23], there are still several obstacles in the way of achieving atomic resolution reconstruction.

To obtain a sufficiently high local electric field (~ 10V/nm), the sample has to be in the form of a sharp needle (radius of curvature $\sim 50-100$nm). However, when atoms are evaporated, the shape of the specimen changes, resulting in local distortions in the electric field, which leads to aberrations in the detector pattern. The situation becomes even more complicated when an inclusion (such as a precipitate of a different species) is present in the otherwise homogeneous matrix. In this case the binding energies may differ notably, meaning that also the critical evaporation field varies between species [16]. This difference will lead to modification of the tip shape, which cannot be predicted from simple geometrical considerations.

Many reconstruction protocols assume that the sample is in the form of a

hemispherical cap on top of a truncated cone [24, 25, 4, 3]. Evaporated ions are assumed to fly off the tip radially, and thus their original positions in the sample are obtained using a simple point projection [24]. A further simplifying assumption is that the sample preserves the "hemisphere on a cone" shape during the whole imaging process, although the radius of curvature is allowed to change.

The ion trajectory is defined by the shape of the electric field above the surface, which means that the shape of the field is of crucial importance for correction of trajectory aberrations. However, it is currently not feasible to conduct *in situ* measurements of surface topology while the APT imaging process is running. Therefore, to obtain the necessary information, computer simulations are often employed. Most simulation techniques rely on solving Laplace's or Poisson's equation to obtain the electric field around the tip under the assumption that the material of the tip is continuous (the effect of individual atoms is not seen) [4, 26] or allowing for atomic resolution by placing the individual atoms on a rigid grid [27, 28, 29, 30]. While valuable information has been obtained using these methods, they rely on approximations which may limit the precision of the obtained results. Moreover, these methods often assume a simple crystallographic structure as well as constrain the movement of atoms.

The simulations presented in this work are performed for either pure Cu or mixed Cu-Fe systems. The choice of materials was motivated by the fact that MD potentials which reproduce several important properties, such as surface energy, elasticity, defect formation energy and mobility [31, 32], exist for these materials, and that Cu is used in a wide range of applications. However, the method can easily be extended to other metallic systems, such as various steels (e.g. Fe-Cr-C [33] and Fe-Cu-Ni [34]) and other alloys (e.g. Al-Mg [35]) for which suitable MD potentials exist.

2. Methods

The HELMOD code [18] is developed based on the classical Molecular Dynamics (MD) code PARCAS [36, 37]. In MD, the motion of individual atoms are calculated by integrating Newton's equations of motion for each atom, enabling realistic simulation of material behavior. In HELMOD the electric field effects are included via interactions with charged surface atoms in addition to the standard interatomic forces of classical MD. The partial charge is induced on surface atoms by an external electric field as a result of interaction of conduction electron density with the local field. The local field around a surface atom is known from the concurrent solution of the Laplace's equation with mixed boundary conditions (Dirichlet at the conducting surface and Neumann in the vacuum), and is recalculated following any change in the surface topology. In this manner the charge on a surface atom can change dynamically depending on the position of the atom with respect to other atoms. In addition to the standard interatomic forces, the Lorenz force acting on the charged surface atoms due to the field as well as the screened Coulomb forces acting between the atoms are considered in HELMOD. The interaction of detached ionized atoms with the external field is ignored since the

external fields are much stronger than the field due to a single elementary charge, and the evaporation events are rare.

The full solution of the Laplace's equation by the finite difference method employed currently in our code becomes a computationally expensive process for a large system with sharp and tall surface features. However, in this case, field evaporation occurs mostly near the apex of the sample, and, thus, the changes in the electric field are also localized to this region. The electric field far away from the apex of the tip is not affected during the evaporation of single atoms, so the calculation of the electric field distribution in the entire system is not required frequently. Instead, at every time step we calculate the field only around the apex in a volume half the size of the total system, while the solution for the full system is calculated e.g. every 20 simulation timesteps, which provides accurate results while maintaining sufficient performance. Between the full solutions, the electrostatic potential is solved only for a volume half the size of the total system, centered at the sample apex. The boundary condition around the smaller grid is set as obtained from the previous full-size grid calculation.

We employ density functional theory (DFT) calculations, using the SIESTA simulation package [38], to verify the correctness of the atomic charges obtained in HELMOD. The calculations are performed using a 256 atom supercell, consisting of 8 {100} FCC layers and a vacuum gap of the same dimensions. Periodic boundary conditions are applied in all directions. Such a geometry provides sufficient room for extra atoms (or vacancies) on one of the surfaces to assess the effect of an electric field. The standard electronic structure was calculated by using the Perdew, Burke & Ernzerhof (PBE) scheme for the exchange and correlation functionals within the generalized gradient approximation (GGA). In our calculations we used the norm-conserving Troullier-Martins pseudopotentials for Cu with $4s^1$ and $3d^{10}$ electrons treated as valence electrons. The partial charge on surface atoms due to the applied electric field is estimated by Mulliken population analysis [39], which gives atomic charge calculated as a sum of electron densities on the valence orbitals of an atom. Since the electron densities are redistributed already due to the formation of the surface and surface defects, we compare the charges on atoms before and after the electric field was applied. We have previously verified by the same method the correctness of the charges obtained in HELMOD for the case of single and double self-adatoms [40].

The low temperatures ($\sim 15-80$K) used in APT slow down considerably all atomic processes, such as surface migration, and thermally assisted field evaporation, taking the time needed for any significant modification in the material structure out of the classical MD timespan. For instance, the time required for a single evaporation event to happen is defined by a typical evaporation frequency, which is 1 event per μs [41], while MD simulations are limited to the ns range. Moreover, in the present form HELMOD does not consider the ionization process itself, which would require additional energy for a surface atom to be able to leave the surface in an ionized state. To cope with these issues we handle the field-assisted evaporation of atoms via a Kinetic Monte Carlo (KMC) [42] step where an atom is picked for evaporation based on a random distribution, which

depends on factors such as binding energy and material dependent properties. In other words, in our code, atoms are allowed to move according to the HELMOD molecular dynamics algorithm at zero temperature, while the removal of atoms in evaporation event is handled by the Monte Carlo step. In this way, the temperature effects are taken into account only via the KMC steps, since the probability P_i of an atom i to be removed by evaporation is proportional to the Boltzmann factor:

$$P_i \propto \nu \exp(-Q_i/k_B T) \tag{1}$$

Here ν is the attempt frequency, Q_i is the evaporation activation energy for the i'th atom, k_B is the Boltzmann constant and T is the sample temperature. This scheme follows the principle of the KMC approach of selecting events stochastically according to their known rates [44, 45, 42]. While it is common to accept the Debye frequency as the attempt frequency ν, we do not aim to provide an actual time scale of the studied process in this work and thus we chose $\nu = 1$ for simplicity.

The electric field required for n-fold ionisation of atom i of element α can be calculated using Müller's evaporation-field formula [47]

$$F_{\mathrm{ev},i} = \frac{4\pi\varepsilon_0}{ne^3} K_i^2. \tag{2}$$

where

$$K_i = \lambda_i + H_{n,\alpha} - n\phi_\alpha \tag{3}$$

and λ_i, $H_{n,\alpha}$ and ϕ_α are the binding energy, energy required for n-fold ionization and work function, respectively. The binding energy is calculated by the MD potential, while the ionization energies and work functions are given as simulation input.

The evaporation activation energy is then given by [48]

$$Q_i = \left[\delta_i^{1/2} + \frac{1}{2}(1-\delta_i)\ln\left((1-\delta_i^{1/2})(1+\delta_i^{1/2})^{-1}\right)\right] K_i. \tag{4}$$

where

$$\delta_i = 1 - F/F_{\mathrm{ev},i}. \tag{5}$$

In the probability calculation, the atom is currently always assumed to be ionized into its most likely state: single ionization for Cu and double ionization for Fe [49]. The work functions are assumed to be constant, $\phi_{\mathrm{Cu}} = 4.5\mathrm{eV}$ and $\phi_{\mathrm{Fe}} = 5.0\mathrm{eV}$ for FCC Fe [50, 51], calculated for the (100) face. We note that the model can be extended in a relatively straightforward manner to deal with higher ionization states. Once an atom has been selected for evaporation, it is removed from the MD system, and its trajectory in the electric field is independently calculated using the velocity Verlet integration scheme [52]. The interaction between an ion and the charged surface atoms is not included in this calculation.

The MD simulation is effectively run as a molecular statics simulation, allowing the structure to relax before the next evaporation event occurs. In our simulation we consider the case $T = 55\mathrm{K}$ which is in the range of temperatures in typical atom probes [46].

All the MD simulations in the current work were performed using the EAM-type Malerba-Pasianot potential which describes well lattice defects and material properties of a mixed Cu-Fe system [31], where the Cu part is based on the potential by Mishin et al. [53] and the Fe part is based on potential by Mendelev et al. [54].

For the reconstruction we employ the second method suggested by Bas et al. in Ref. [24]. The method utilizes a point projection to determine the original position of atoms, accounting for the curvature of the reconstructed sample.

3. Simulations

To demonstrate the usefulness of the new method, we simulated four different samples: a) a flat Cu surface, b) a flat Cu surface with a Fe inclusion, c) a flat Cu surface with a small pit of diameter 2nm, d) a Cu tip of the type "hemisphere-on-a-post" (Figure 1). In cases a)-c) the size of the simulated system was $7.2\text{nm} \times 7.2\text{nm} \times 5.4\text{nm}$. In case b) an FCC Fe inclusion was inserted into the matrix by replacing the Cu atoms with Fe atoms within a hemispherical volume with radius 2.7nm at the surface. Due to the small size of the inclusion the Fe lattice repeats the Cu FCC lattice [55]. In case c) the atoms in the same volume as case b) were simply removed to create a pit. No Fe is placed in the surrounding Cu matrix to simplify analysis. While the low Fe-concentration in the matrix would lead to long-term evolution of the Fe-precipitate, the timescale for such effects is longer than the time considered in the simulation. Case d) consisted of a tip of height 15nm, shank angle 7° and an initial radius of curvature 1.0nm at the apex. It is worth noting that this value, chosen for computational reasons, is much smaller than for samples commonly used in atom probes. In all cases the surface normal was in the {100}-direction. The two bottom atomic layers were fixed, and periodic boundaries were used at the sides. In cases a)-c) the maximum applied field was 13V/nm which was ramped linearly over a time period of 32.5ps. The ramping of the field is necessary to avoid the sudden introduction of a very large force on the surface atoms, which may result in surface oscillation [56]. The field value was chosen as to be low enough not to cause spontaneous evaporation due to the MD algorithm after field enhancement is accounted for, while still being high enough to enable realistic dynamics under a high field. In case d) the applied field was at a maximum 1.0V/nm ramped over 4.5ps, which corresponds to a locally enhanced field of similar magnitude as the previous cases.

Although the structures a)-c) are not in the shape of sharp needles, commonly used in the APT measurements, the simple geometry eases the analysis of the results with the purpose to isolate the causes for aberrations. These cases may also be seen as representing the tip of a sample with a large radius of curvature at the apex.

4. Results

The grid used in the Laplace's solver consists of fairly coarse grid points as each grid point is at least the size of a single atom. While aiming to study the effect of point

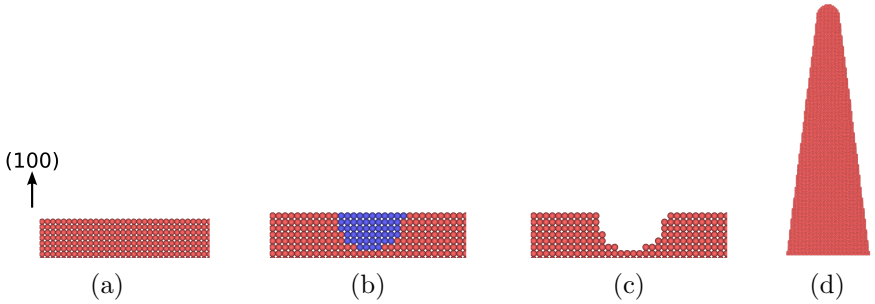

Figure 1: (Color online) 2D slices of the 3D simulation inputs used in this paper as viewed from the side. a) a flat Cu-surface, b) a flat Cu surface with a small Fe inclusion, c) a flat Cu surface with a small pit, and d) a Cu tip of the type hemisphere-on-a-post.

Defect	HELMOD	DFT	Relative difference
1 adatom	0.043e	0.034e	+26%
2 adatoms	0.035e	0.025e	+40%
4 adatoms	0.026e	0.023e	+13%
5 adatoms	0.058e	0.055e	+5%
1 vacancy	0.009e	0.009e	0%
2 vacancies	0.010e	0.010e	0%
4 vacancies	0.015e	0.011e	+36%

Table 1: Charge induced on adatoms or around vacancies on a otherwise flat Cu surface with an applied field of 2V/nm, as calculated via the HELMOD algorithm used in this paper, and DFT as implemented in the SIESTA package [38]. In the case of 1-4 adatoms the adatoms are located next to each other, while in the case of 5 adatoms one adatom is located in a layer above four adatoms.

defects it is important to analyze the sensitivity of such calculations. We performed the comparison between the HELMOD and SIESTA results of the partial charge induced on a adatoms, or atoms surrounding a vacancy or vacancy cluster, in the presence of an applied external electric field with magnitude 2V/nm (Table 1). The results show that the value obtained via the HELMOD algorithm agrees fairly well with the DFT calculations, which further shows that this approach is a valid way to calculate the charge of surface atoms.

Fig. 2 shows the simulated impact positions on a detector for cases a)-c). It is seen that for case a) with just a smooth surface, the pattern is fairly regular and reflects the underlying crystal structure, although discrepancies are clearly visible. The detector images for both cases with a pit (case b) and with a Fe inclusion (case c) look similar, as only few atoms are detected in the center where the pit or inclusion is located. The electric field inside the pit is weaker than at the top surface, and, thus, few atoms are evaporated from inside the pit. In the case of the inclusion, Fe has a higher evaporation

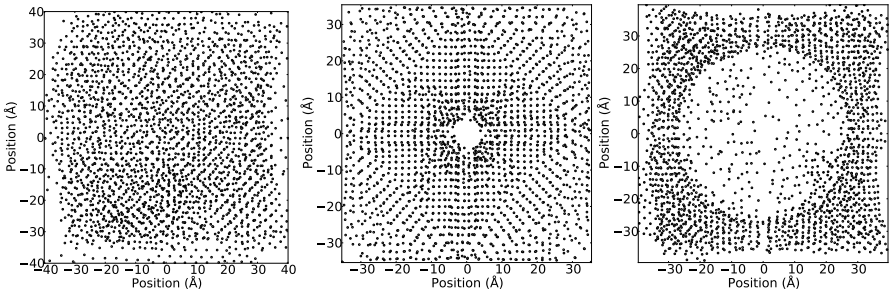

(a) (b) (c)

Figure 2: Simulated detector hits in the case of a) flat Cu surface b) flat Cu surface with a pit and c) flat Cu surface with an Fe inclusion. The total number of evaporation events in all three cases is 2400, corresponding to 3 atomic monolayers in the simulation cell.

field than the surrounding Cu matrix ($F_{\mathrm{ev,Cu}} \approx 30\mathrm{V/nm}$ for Cu and $F_{\mathrm{ev,Fe}} \approx 33\mathrm{V/nm}$ for Fe), and, thus, the Cu is preferentially evaporated around the inclusion, leaving a Fe protrusion behind (fig. 3). This protrusion distorts the electric field in such a way that trajectories of the atoms evaporating from the protrusion point away from the centre, resulting in a similar detection pattern as in the case of a pit. It can, thus, be difficult to distinguish these two cases from each other based on detector data, even though the underlying structures are very different. The relaxation process along with the local enhancement of the field at the protrusion, promote the Fe atoms to be displaced upward, increasing the size of the protrusion and enlarging further the enhancement of the electric field around it.

Our method allows us to analyze the limitation of reconstruction algorithms. For instance, when reconstructing APT data, the initial depth of a detected atom is calculated from the evaporation order. For this to work, it is assumed that the evaporation order is well defined, and that atoms evaporate one layer at a time. However, as fig. 4 shows, this is not always the case. For instance, the atoms from the flat surface with the Fe inclusion are initially evaporating from the top atomic layer, with most of the Fe atoms belonging to a layer being the last to evaporate. However, some of the Fe atoms from the top layer do not evaporate until after the Cu atoms in the next layer. Because the Fe atoms are evaporating later than the Cu atoms of the same layer, a reconstruction would show them as coming from deeper below the surface layers than they truly are. In fact the opposite is true, because the remaining Fe atoms in the layer form a protrusion, the electric field strength is enhanced above it, pulling the Fe atoms upwards, as seen in fig. 3.

Another limitation is the assumption of homogeneity of the electric field distribution. In the presence of a homogeneous electric field, the trajectories of evaporated atoms follow the surface normal. However, after each evaporation event, the surface geometry changes slightly, giving rise to variations in the local electric field.

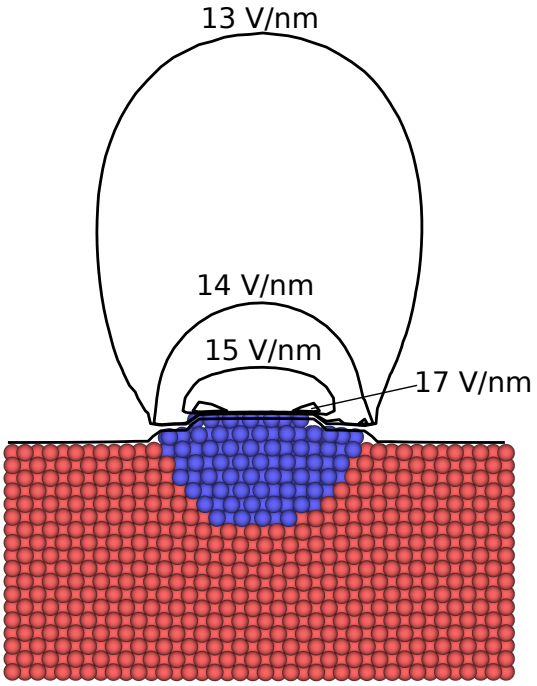

Figure 3: (Color online) An Fe protrusion is formed when the Cu surrounding an Fe inclusion is evaporated before the Fe. The electric field is then distorted and enhanced around the protrusion.

This, in turn, causes aberrations in trajectories of evaporating atoms at neighbouring sites. Fig. 5 shows the deviations of tracks from the surface normal of an initially flat surface. On average the trajectories deviate 4.7° from the expected. This shows that even when only a few atoms are missing, the change in the electric field is large enough to produce visible aberrations in trajectories. However, the deviation is markedly higher for the last atoms of a layer to evaporate, due to the formation of a Fe protrusion distorting the electric field (Figure 3).

Finally, we reconstructed the image of the tip from the simulated detector data, which is shown in Fig. 6 for case d), the tip. The crystallographic structure of the tip is visible in the detector pattern. Fig. 7a shows the original tip which is simulated, while fig. 7b shows the reconstruction based on the simulated detector data (using the algorithm by Bas et al. [24]). The reconstruction is similar in size and shape as the original tip. However, it can be seen that there is intermixing of layers in the reconstructed tip, with e.g. some atoms that were located near the tip apex being erroneously placed further down in the reconstruction. The problem is especially apparent at the tip apex. Moreover, even though the initial structure is a perfect single crystal, the reconstructed image does not show any trace of the underlying crystalline structure.

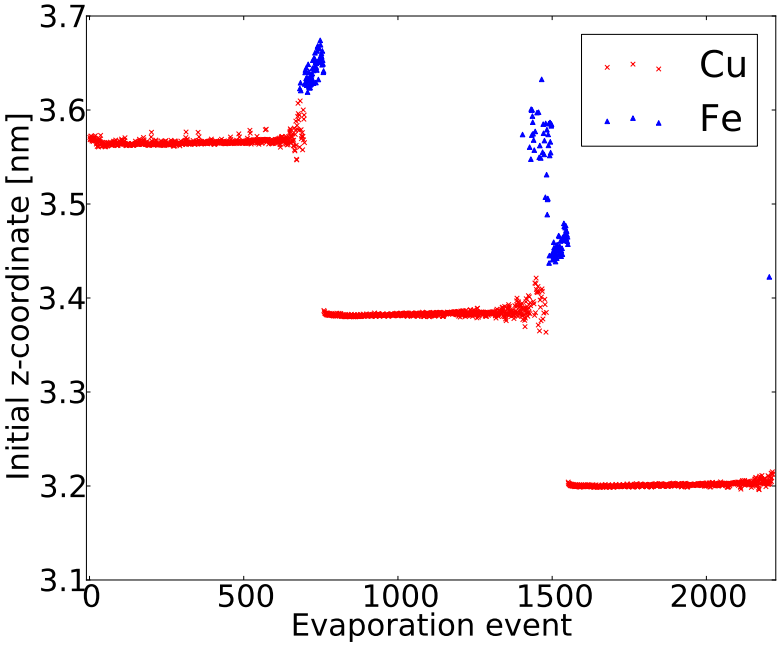

Figure 4: (Color online) The initial height-position of evaporated atoms in the case of a Fe inclusion in a Cu matrix. Atoms are mostly evaporating one layer at a time, with some mixing of layers occurring. The matrix surrounding the inclusion is evaporated preferentially. Red crosses correspond to evaporated Cu ions, and blue triangles to Fe ions.

5. Conclusions

In the present work, we present a new method to simulate APT processes, based on concurrent electrodynamic-molecular dynamic simulations with the addition of a KMC step to handle evaporation of ions at cryogenic temperatures. The method combines the accuracy of molecular dynamics with the computational efficiency of a Monte Carlo algorithm, and thus enables simulating the processes occurring in APT with high reliability. The method opens up new avenues of investigating the effects of field evaporation in atom probes, as there are no other tools with the same set of features, such as including full surface dynamics, in wide use currently. Using the code it is possible to benchmark reconstruction algorithms, as it is possible to easily compare the obtained reconstructions with the perfectly known initial structure.

Using our simulation code we have shown that already the simplest case of a flat surface reveals a large problem in many current APT reconstruction methods: it is difficult to account for the small atomic-scale local variations in the electric field, which occur when atoms evaporate from the surface and can affect reconstructions. The main aberrations seen in our simulation are the modification of ion trajectories due to small distortions in the local electric field at the surface, and the intermixing of layers due

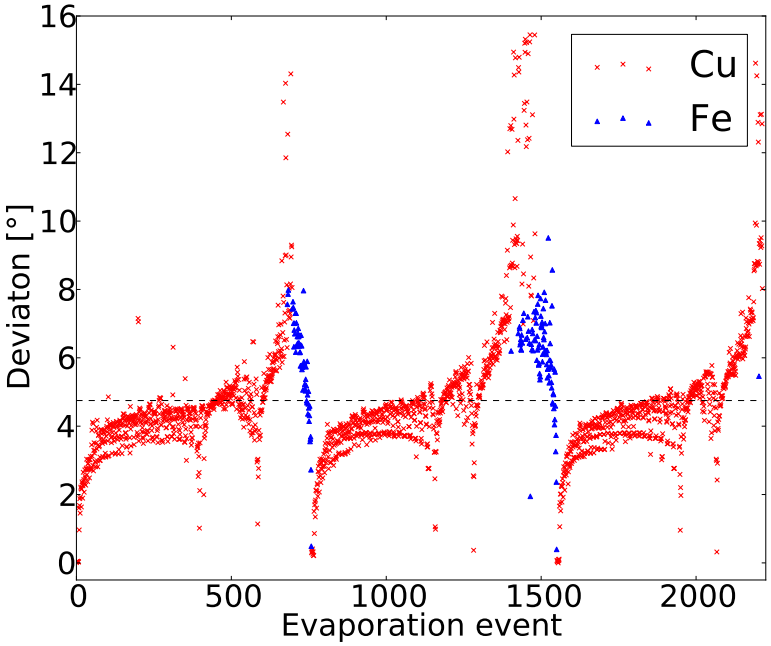

Figure 5: (Color online) Deviation of trajectories of evaporated atoms from the surface normal of an initially flat surface with an Fe inclusion. In the case of a completely flat surface and a homogeneous electric field the deviations should be 0°. The large peaks correspond to the situations were a Fe protrusion has formed on the surface, distorting the electric field around it. These peaks are periodic, and approximately correspond to the evaporation of one monolayer from the surface. The dashed line indicates the average deviation. Red crosses correspond to evaporated Cu ions, and blue triangles to Fe ions.

to out-of-order evaporation events. It is also difficult to distinguish between inclusions and pits on a surface, resulting in identical detection patterns. These factors place limits on the accuracy of APT reconstructions which are independent of the detector sensitivity. The performed analysis indicates that the existing reconstruction algorithms are not capable to always predict precisely the atomic composition and constitution of the material under investigation, due to the insufficient information on material surface behavior under high electric fields.

In addition to benchmarking current reconstruction algorithms, our simulation approach can also be used to develop and calibrate improved APT reconstruction algorithms, such as statistical algorithms based on Bayesian inversion [57]. In this approach reconstructions are guided by knowledge of "likely correct" reconstructions based on a large number of simulation results, obtained by the simulation code described in this work. These kind of statistical reconstruction algorithms may perform better than current algorithms, as they implicitly include effects like the one described above, instead of modeling them in the reconstruction algorithms themselves.

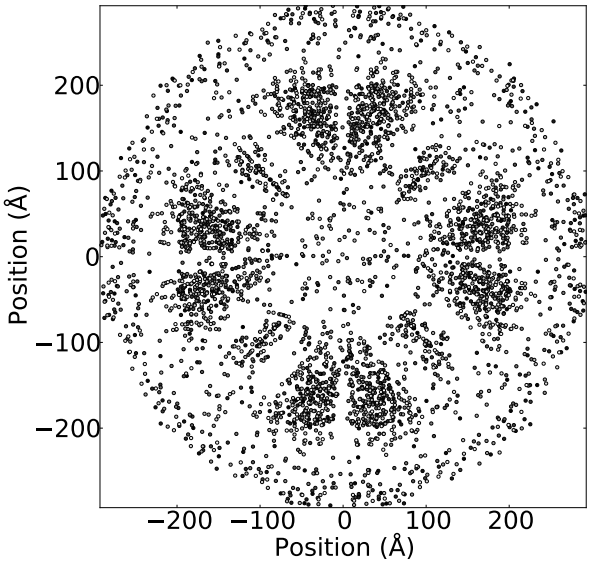

Figure 6: Impact positions on detector from the simulated APT sample. The detector data is used as input for the reconstruction algorithm. The total number of evaporation events is 3860.

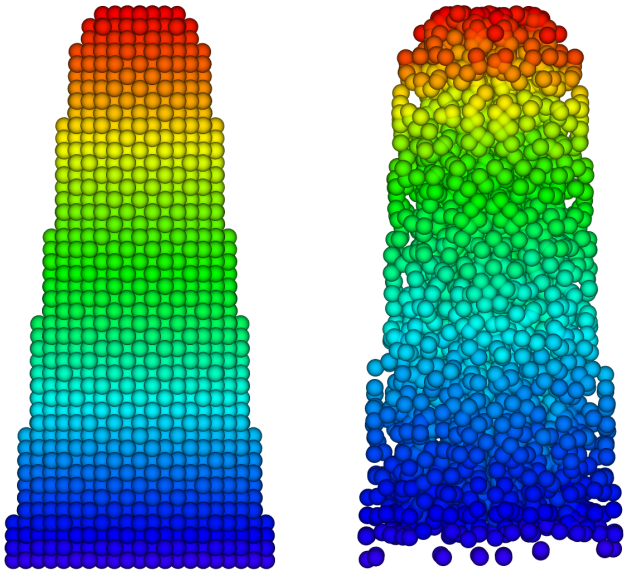

Figure 7: (Color online) Part of the original tip and the reconstructed model based on 3860 evaporation events. The color indicates the original coordinate of an atom along the main axis of the tip.

6. Acknowledgements

We gratefully acknowledge the discussions with C. Müller and Dr. Stephan Gerstl of ETH Zürich, and Prof E. Marquis of the University of Michigan. This research was funded by the European Commission under the FP7 Research Infrastructures project EuCARD (grant no. 227579) and The Academy of Finland project AMELIS. Computing resources were provided by the Finnish IT Center for Science (CSC).

[1] E. A. Marquis, B. P. Geiser, T. J. Prosa, and D. J. Larson. Evolution of tip shape during field evaporation of complex multilayer structures. *J. Microsc.*, 241(3):225–233, 2011.

[2] F. Vurpillot, M. Gruber, G. Da Costa, I. Martin, L. Renaud, and A. Bostel. Pragmatic reconstruction methods in atom probe tomography. *Ultramicroscopy*, 111(8):1286–1294, July 2011.

[3] Francois Vurpillot, Baptiste Gault, Brian P. Geiser, and D. J. Larson. Reconstructing atom probe data: A review. *Ultramicroscopy*, 132:19–30, September 2013.

[4] B. Gault, D. Haley, F. de Geuser, M. P. Moody, E. A. Marquis, D. J. Larson, and B. P. Geiser. Advances in the reconstruction of atom probe tomography data. *Ultramicroscopy*, 111(6):448–457, May 2011.

[5] D. Vaumousse, A. Cerezo, and P. J. Warren. A procedure for quantification of precipitate microstructures from three-dimensional atom probe data. *Ultramicroscopy*, 95:215–221, May 2003.

[6] F. De Geuser, W. Lefebvre, F. Danoix, F. Vurpillot, B. Forbord, and D. Blavette. An improved reconstruction procedure for the correction of local magnification effects in three-dimensional atom-probe. *Surf. Interface Anal.*, 39(2-3):268–272, 2007.

[7] Emmanuelle A. Marquis and Francois Vurpillot. Chromatic aberrations in the field evaporation behavior of small precipitates. *Microscopy and Microanalysis*, 14(06):561–570, December 2008.

[8] Mukesh Bachhav, G. Robert Odette, and Emmanuelle A. Marquis. precipitation in neutron-irradiated FeCr alloys. *Scripta Materialia*, 74:48–51, March 2014.

[9] Keith Thompson, John H. Booske, David J. Larson, and Thomas F. Kelly. Three-dimensional atom mapping of dopants in si nanostructures. *Appl. Phys. Lett.*, 87(5):052108+, 2005.

[10] K. Inoue, F. Yano, A. Nishida, H. Takamizawa, T. Tsunomura, Y. Nagai, and M. Hasegawa. Dopant distributions in n-MOSFET structure observed by atom probe tomography. *Ultramicroscopy*, 109(12):1479–1484, November 2009.

[11] J. S. Moore, K. S. Jones, H. Kennel, and S. Corcoran. 3-D analysis of semiconductor dopant distributions in a patterned structure using LEAP. *Ultramicroscopy*, 108(6):536–539, May 2008.

[12] Thomas F. Kelly, Patrick P. Camus, David J. Larson, Louis M. Holzman, and Sateesh S. Bajikar. On the many advantages of local-electrode atom probes. *Ultramicroscopy*, 62(1-2):29–42, January 1996.

[13] G. L. Kellogg and T. T. Tsong. Pulsed-laser atom-probe field-ion microscopy. *J. Appl. Phys.*, 51(2):1184–1193, 1980.

[14] Baptiste Gault, Emmanuelle A. Marquis, David W. Saxey, Gareth M. Hughes, Dominique Mangelinck, Eric S. Toberer, and G. Jeff Snyder. High-resolution nanostructural investigation of Zn4Sb3 alloys. *Scr. Mater.*, 63(7):784–787, October 2010.

[15] Fengzai Tang, Baptiste Gault, Simon P. Ringer, and Julie M. Cairney. Optimization of pulsed laser atom probe (PLAP) for the analysis of nanocomposite TiSin films. *Ultramicroscopy*, 110(7):836–843, June 2010.

[16] Joaquín Peralta, Scott R. Broderick, and Krishna Rajan. Mapping energetics of atom probe evaporation events through first principles calculations. *Ultramicroscopy*, 132:143–151, September 2013.

[17] G. Da Costa, F. Vurpillot, A. Bostel, M. Bouet, and B. Deconihout. Design of a delay-line position-sensitive detector with improved performance. *Review of Scientific Instruments*, 76(1):013304+,

January 2005.

[18] F. Djurabekova, S. Parviainen, A. Pohjonen, and K. Nordlund. Atomistic modeling of metal surfaces under electric fields: Direct coupling of electric fields to a molecular dynamics algorithm. *Phys. Rev. E*, 83:026704+, February 2011.

[19] Ilke Arslan, Emmanuelle A. Marquis, Mark Homer, Michelle A. Hekmaty, and Norman C. Bartelt. Towards better 3-D reconstructions by combining electron tomography and atom-probe tomography. *Ultramicroscopy*, 108(12):1579–1585, November 2008.

[20] Michael P. Moody, Baptiste Gault, Leigh T. Stephenson, Ross K. W. Marceau, Rebecca C. Powles, Anna V. Ceguerra, Andrew J. Breen, and Simon P. Ringer. Lattice rectification in atom probe tomography: Toward true Three-Dimensional atomic microscopy. *Microsc. Microanal.*, 17(02):226–239, 2011.

[21] Moody Michael, Ceguerra Anna, Breen Andrew, Cui X. Yuan, Gault Baptiste, Stephenson Leigh, Marceau Ross, Powles Rebecca, and Ringer Simon. Atomically resolved tomography to directly inform simulations for structureproperty relationships. *Nat Commun*, 5, November 2014. Supplementary information available for this article at http://www.nature.com/ncomms/2014/141119/ncomms6501/suppinfo/ncomms6501_S1.html.

[22] Michael P. Moody, Baptiste Gault, Leigh T. Stephenson, Daniel Haley, and Simon P. Ringer. Qualification of the tomographic reconstruction in atom probe by advanced spatial distribution map techniques. *Ultramicroscopy*, 109(7):815–824, June 2009.

[23] L. Yao, M. P. Moody, J. M. Cairney, Daniel Haley, A. V. Ceguerra, C. Zhu, and S. P. Ringer. Crystallographic structural analysis in atom probe microscopy via 3D hough transformation. *Ultramicroscopy*, 111(6):458–463, May 2011.

[24] P. Bas, A. Bostel, B. Deconihout, and D. Blavette. A general protocol for the reconstruction of 3D atom probe data. *Appl. Surf. Sci.*, 87-88:298–304, March 1995.

[25] B. P. Geiser, D. J. Larson, E. Oltman, S. Gerstl, D. Reinhard, T. F. Kelly, and T. J. Prosa. Wide-Field-of-View atom probe reconstruction. *Microsc. Microanal.*, 15(Supplement S2):292–293, 2009.

[26] Daniel Haley, Michael P. Moody, and George D. W. Smith. Level set methods for modelling field evaporation in atom probe. *Microsc. Microanal.*, 19:1–9, August 2013.

[27] Vurpillot, Bostel, and Blavette. The shape of field emitters and the ion trajectories in three-dimensional atom probes. *J. Microsc.*, 196(3):332–336, 1999.

[28] F. Vurpillot, A. Bostel, and D. Blavette. Trajectory overlaps and local magnification in three-dimensional atom probe. *Appl. Phys. Lett.*, 76(21):3127–3129, 2000.

[29] Christian Oberdorfer and Guido Schmitz. On the field evaporation behavior of dielectric materials in Three-Dimensional atom probe: A numeric simulation. *Microsc. Microanal.*, 17(01):15–25, 2011.

[30] Christian Oberdorfer, Sebastian M. Eich, and Guido Schmitz. A full-scale simulation approach for atom probe tomography. *Ultramicroscopy*, 128:55–67, May 2013.

[31] R. C. Pasianot and L. Malerba. Interatomic potentials consistent with thermodynamics: The FeCu system. *J. Nucl. Mater.*, 360(2):118–127, February 2007.

[32] B. Jelinek, S. Groh, M. F. Horstemeyer, J. Houze, S. G. Kim, G. J. Wagner, A. Moitra, and M. I. Baskes. Modified embedded atom method potential for al, si, mg, cu, and fe alloys. *Phys. Rev. B*, 85:245102, June 2012.

[33] K. O. E. Henriksson, C. Björkas, and K. Nordlund. Atomistic simulations of stainless steels: a many-body potential for the Fe–Cr–C system. *Journal of Physics: Condensed Matter*, 25(44):445401, 2013.

[34] G. Bonny, R. C. Pasianot, N. Castin, and L. Malerba. Ternary FeCuni many-body potential to model reactor pressure vessel steels: First validation by simulated thermal annealing. *Philosophical Magazine*, 89(34-36):3531–3546, December 2009.

[35] M. I. Mendelev, M. Asta, M. J. Rahman, and J. J. Hoyt. Development of interatomic potentials appropriate for simulation of solidliquid interface properties in AlMg alloys. *Philosophical*

Magazine, 89(34-36):3269–3285, December 2009.

[36] K. Nordlund, M. Ghaly, R. S. Averback, M. Caturla, T. Diaz de la Rubia, and J. Tarus. Defect production in collision cascades in elemental semiconductors and fcc metals. *Phys. Rev. B*, 57(13):7556–7570, 1998.

[37] M. Ghaly, K. Nordlund, and R. S. Averback. Molecular dynamics investigations of surface damage produced by kev self-bombardment of solids. *Phil. Mag. A*, 79(4):795, 1999.

[38] José M. Soler, Emilio Artacho, Julian D. Gale, Alberto García, Javier Junquera, Pablo Ordejón, and Daniel. The SIESTA method for ab initio order-N materials simulation. *J. Phys.: Condens. Matter*, 14(11):2745–2779, March 2002.

[39] R. S. Mulliken. Electronic population analysis on lcaomo molecular wave functions. ii. overlap populations, bond orders, and covalent bond energies. *J. Chem. Phys.*, 23(10):1841–1846, 1955.

[40] Flyura Djurabekova, Avaz Ruzibaev, Eero Holmström, Stefan Parviainen, and Mikko Hakala. Local changes of work function near rough features on cu surfaces operated under high external electric field. *J. Appl. Phys.*, 114(24), 2013.

[41] Maria Gruber, François Vurpillot, Alain Bostel, and Bernard Deconihout. Field evaporation: A kinetic monte carlo approach on the influence of temperature. *Surf. Sci.*, 605(23-24):2025–2031, December 2011.

[42] K. A. Fichthorn and W. H. Weinberg. Theoretical foundations of dynamical monte carlo simulations. *J. Chem. Phys.*, 95(2):1090–1096, July 1991.

[43] Erwin W. Müller. Field desorption. *Phys. Rev.*, 102:618–624, May 1956.

[44] W. M. Young and E. W. Elcock. Monte carlo studies of vacancy migration in binary ordered alloys: I. *Proc. Phys. Soc.*, 89(3):735–746, November 1966.

[45] A. B. Bortz, M. H. Kalos, and J. L. Lebowitz. A new algorithm for monte carlo simulation of ising spin systems. *J. Comput. Phys.*, 17(1):10–18, January 1975.

[46] Thomas F. Kelly, David J. Larson, Keith Thompson, Roger L. Alvis, Joseph H. Bunton, Jesse D. Olson, and Brian P. Gorman. Atom probe tomography of electronic materials. *Annu. Rev. Mater. Res.*, 37(1):681–727, 2007.

[47] Erwin W. Müller. Field desorption. *Phys. Rev.*, 102:618–624, May 1956.

[48] Richard G. Forbes. Field evaporation theory: a review of basic ideas. *Appl. Surf. Sci.*, 87-88:1–11, March 1995.

[49] Tien T. Tsong. *Atom-Probe Field Ion Microscopy: Field Ion Emission, and Surfaces and Interfaces at Atomic Resolution*. Cambridge University Press, 2005.

[50] P. O. Gartland, S. Berge, and B. J. Slagsvold. Photoelectric work function of a copper single crystal for the (100), (110), (111), and (112) faces. *Phys. Rev. Lett.*, 28(12):738–739, 1972.

[51] C. L. Fu and A. J. Freeman. Electronic and magnetic properties of the fcc fe(001) thin films: Fe/Cu(001) and Cu/Fe/cu(001). *Phys. Rev. B*, 35:925–932, 1987.

[52] Loup Verlet. Computer "experiments" on classical fluids. i. thermodynamical properties of Lennard-Jones molecules. *Phys. Rev.*, 159(1):98–103, July 1967.

[53] Y. Mishin, M. J. Mehl, D. A. Papaconstantopoulos, A. F. Voter, and J. D. Kress. Structural stability and lattice defects in copper: Ab initio, tight-binding, and embedded-atom calculations. *Phys. Rev. B*, 63(22):224106, May 2001.

[54] M. I. Mendelev, S. Han, D. J. Srolovitz, G. J. Ackland, D. Y. Sun, and M. Asta. Development of new interatomic potentials appropriate for crystalline and liquid iron. *Philosophical Magazine*, 83(35):3977–3994, December 2003.

[55] Y. Tsunoda and N. Kunitomi. Structural phase transition of -Fe precipitates in cu. *Journal of Physics F: Metal Physics*, 18(7):1405+, July 1988.

[56] A. S. Pohjonen, F. Djurabekova, K. Nordlund, A. Kuronen, and S. P. Fitzgerald. Dislocation nucleation from near surface void under static tensile stress in cu. *J. Appl. Phys.*, 110(2):023509+, July 2011.

[57] J. Kaipio and E. Somersalo. *Statistical and Computational Inverse Problems*, volume 160 of *Applied Mathematical Sciences*. Springer Verlag, 2004.